RESEARCH REPORT

VTT-R-00041-26

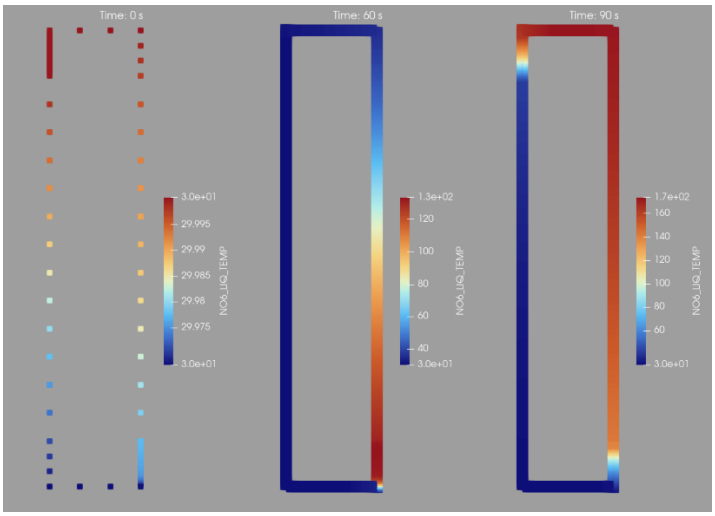

Apros natural circulation in SMR-like geometries

Authors: Seppo Hillberg

Confidentiality: VTT Public

Version: 30.01.2026

Report's title	
Apros single-phase flow stability in SMR-like geometries	
Customer, contact person, address	**Order reference**
SAFER2028, Juha Luukka, STUK	SAFER 12/2025
Project name	**Project number/Short name**
Analysis of Passive Safety Systems' Operations and Modelling	141373 / ESPO
Author(s)	**Pages**
Seppo Hillberg	35/
Keywords	**Report identification code**
natural circulation, SMR, single-phase, instability	VTT-R-00041-26

Summary

Apros is widely used in simulation of varied natural circulation geometries, including SMRs. Even when a system operates far from boiling conditions, single phase flow in a SMR-type geometry may exhibit oscillations and flow reversals. Even if the system is ultimately stable in all flow regimes, these temporary oscillations may contribute to control and protection challenges – and in long term even to metal fatigue.

Apros natural circulation has been tested in rectangular closed loop geometry using 5 different loop heights, 3 different nodalization, 4 different loop flow resistances and using three different test types. In total 240 single phase simulations were performed, of which tested a total of 840 states. All the tested cases proved ultimately stable.

The reviewed simulation set revealed nothing suspicious in Apros' capability in modelling natural circulation of SMR designs. Unrealistic behaviour seen in some of the tests can be attributed to too simple nodalization. The simulations highlighted the potential for user error when trying to over-simplify geometries that encounter three-dimensional flow patterns, especially at very low powers.

Confidentiality	VTT Public

Espoo 30.1.2026

Written by	**Reviewed by**
Seppo Hillberg, Senior Scientist	Jukka Röppänen, Senior Solutions Scientist

VTT's contact address

VTT Technical Research Centre of Finland Ltd, P.O. Box 1000, FI-02044 VTT, Finland.

Distribution (customer and VTT)

by email to SAFER2028 Technical Advisory Group 2.1 (TAG 2.1).

Approval

VTT TECHNICAL RESEARCH CENTRE OF FINLAND LTD

Date:	09 March 2026
Signature:	DocuSigned by: 7CF631A9E3CE476...
Name:	Joona Kurki
Title:	Research Team Leader

Preface

The key driver for this report was the increasing interest in natural circulation SMR's and the role of Apros in analysing them. While there isn't any particular reason to suspect Apros wouldn't be suitable for modelling the required phenomena, this topic hasn't been as widely tested as it could be. Since I, the modeller, wanted to test multiple configurations and nodalizations using very simplified geometry, a deep dive into any specific SMR-configuration was not possible. Therefore, using layman's terms, I decided to shake Apros models of different geometries and see if anything breaks loose in the calculation.

Espoo 30.1.2026

Seppo Hillberg

Contents

1. Introduction

Apros is widely used in simulation of varied natural circulation geometries, including SMRs. Even when a system operates far from boiling conditions, single phase flow in a SMR-type geometry may exhibit oscillations and flow reversals. Even if the system is ultimately stable in all flow regimes, these temporary oscillations may contribute to control and protection challenges – and in long term even to metal fatigue.

This report does not focus on one single geometry but instead tries to overview a range of SMR-like geometries. The focus is limited on single-phase phenomena and vertical heater and cooler. Since the cases cannot be compared to experimental data, this assessment relies on expert judgement to assess the realism of the simulated behaviour.

Main object of the work was to study if Apros solution of natural circulation in selected geometries encounters instabilities of numerical or physical origin. Secondary goal was to discover how nodalization, flow losses and used heating power affect system response.

2. A look into experimental and theoretical background

One of the inspirations for this review is a Nuscale natural circulation stability study [1] which mentions that oscillatory instability is possible if feedback is negative, delayed and sufficiently strong. They conclude that in their concept:

- Feedback is negative since increase in flow decreases core exit temperature
- Feedback is delayed since there is delay in circulation. Density differences move at a limited speed.
- Feedback varies depending on situation

One of the inspirations for the Nuscale presentation seems to have been a paper by Pilkhwal et. al [2] which discusses four different heating-cooling configurations that were tested in a rectangular loop in BARC facility [3]. In these experiments the only unstable geometry had of horizontal heaters and coolers. All other combinations of vertical/horizontal heater & cooler combinations were found to be stable.

P. K. Vijayan et al. studied loop diameter glass-made test loops [4] with horizontal heat exchangers. They concluded that for single phase flow, increasing loop diameter had destabilizing effect on the system.

Instability lecture by F. D. Auria et al. [5] covers some historical examples and explains basics. With multiple references it mentions that heat capacity affects stability of the flow. This is rather intuitive since fixed amount of energy stored only to fluid vs. fluid & wall leads to different fluid temperature and energy stored in the walls will dissipate to water over a time.

IAEA-TECDOC-1474 [6] points out that due to nonlinear nature of circulation instabilities are much more likely in natural circulation system than in forced circulation system. It also points out that due to low driving force, the stabilizing effect of inlet orifices is limited.

In general, the conclusions of reviewed literature suggest that single-phase instabilities are more probable in tall systems with large flow area, low flow resistance, thin walls and low driving force. Horizontal heater – horizontal cooler arrangements are most prone to instabilities while vertical-vertical systems are most stable.

3. Apros model and test setup

3.1 Simulation model

Apros model of the circulation loop is shown in the Figure 1. This model was used as a base for 15 total height and nodalization combinations. Circulation loop total height and flow length of the nodes was varied between the simulation cases. Total loop height was varied from 10 to 30 m and node target length from 0.1 m to 1.0 m. Exception to loop nodalization were the heating and cooling sections, which had fixed geometry and nodalization. The circulation loop is presented in Tables Table 1 and Table 2. Varied geometries are presented in Table 3.

Apart from heating and cooling sections, the other sections of the loop didn’t have walls. This was done to provide as favourable as possible conditions for any instabilities since heat capacities along

the flow path would act to dampen in the oscillations. For the same reason surface absolute roughness was set as very smooth (0.01 mm).

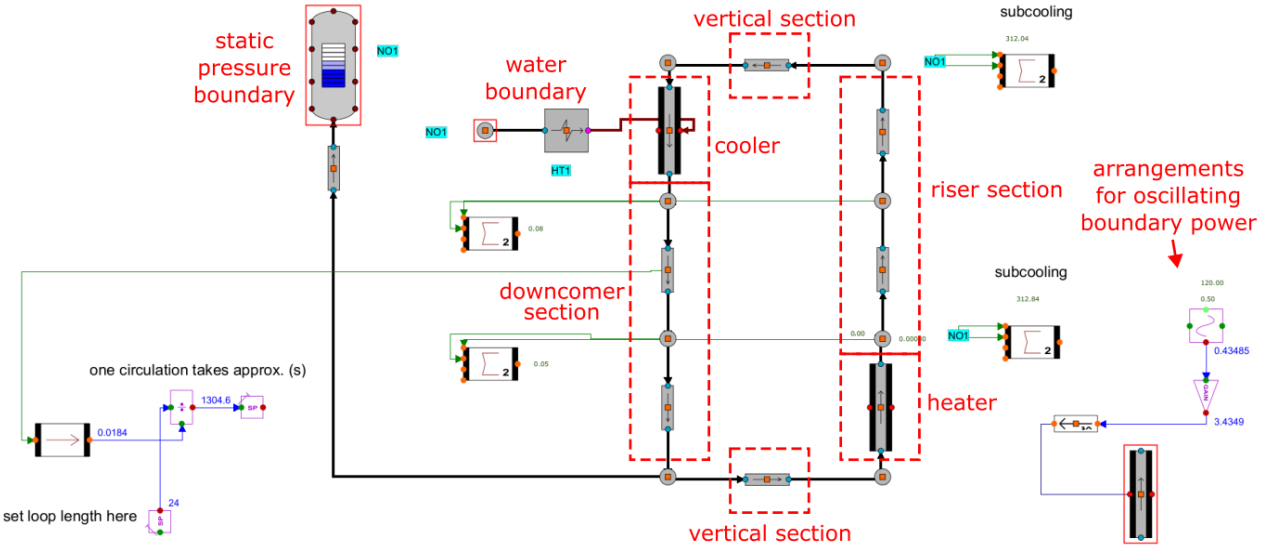

Figure 1. Apros model of the circulation loop. Used expansion tank was excluded and used as a static pressure boundary. Heating section as at bottom right and cooling section is at top left. Positive circulation is counter-clockwise. Geometry variations were read into the model from SCL scripts.

Table 1. Description of modelled circulation loop (parts without external heat transfer)

Attribute	**Value**
total height	variable
length of vertical sections	2 m
total flow length	variable (based on total height and length of vertical sections)
number of calculation nodes in system	variable
inner diameter[1]	0.1 m
flow area	0.007854 m^2
used process component	pipe (no walls)

[1] Diameter was intended to be 0.5 m, which results to same flow area as in the heat exchangers, but due to an error 0.1 m diameter ended up being used in all the simulations.

additional losses	form loss 0.2 in all 6 pipe sections
pressure control	150 bar(abs) static pressure boundary

Table 2. Description of heating and cooling sections of circulation loop

Attribute	**Value**
length	1.5 m
number of calculation nodes	30
type of heat exchanger	heat pipe
orientation	vertical
material	stainless steel
number of heat exchanger tubes	1111
inner diameter of heat exchanger tubes	1.5 cm
tube wall thickness	1 mm
total flow area	0.19633 m^2
boundary connected to heat exchanging wall structure	specified heating power of tube walls (heater) / excluded water node at 30 °C (cooler)
form loss	variable

Table 3. Geometry & nodalization combinations and corresponding identification numbers.

geometry id	loop height (m)	node target length (m)	number of nodes	total loop length (m)	heater-cooler center elevation dist. (m)
1	10	0.1	278	24	8.5
2	15	0.1	378	34	13.5
3	20	0.1	478	44	18.5
4	25	0.1	578	54	23.5
5	30	0.1	678	64	28.5
11	10	0.5	110	24	8.5
12	15	0.5	130	34	13.5
13	20	0.5	150	44	18.5
14	25	0.5	170	54	23.5
15	30	0.5	190	64	28.5
21	10	1	90	24	8.5
22	15	1	100	34	13.5
23	20	1	110	44	18.5
24	25	1	120	54	23.5
25	30	1	130	64	28.5

3.2 Simulation test matrix

Simulation test matrix consisted of three types of tests (Table 4) aimed to test natural circulation in different scenarios. Within test types, variables were flow loss of the circulation loop and heating power. Flow loss was adjusted by adding a form loss coefficient to both the heating and cooling sections. All the tests were subcooled.

Transient cases of Table 5 were applied to all of the geometry configurations presented in Table 3. This resulted to 240 simulations. Geometries and transients have unique identifiers and later in this report they are referred as calculation case combinations like “g1t1” – first geometry id together with the first transient id.

Table 4. Test types for simulations.

Transient type	**Description**
Hot water pulse in cold system	Initial state is at 30 °C with no flow. Heating is applied at 3 MW for 60 s. Cooling is active throughout the simulation. Simulation ends at 5000 seconds.
Flow initiation	Initial state is at 30 °C with no flow. Heating is applied at specified power. Heating and cooling are active throughout the simulation. Simulation ends at 5000 seconds.
Sine wave heating power (3 MW ± 0.5 MW)	Initial state is steady state at 3 MW. Sine wave tests consist of 11 steps in which heating power is modified with a 500 kW amplitude sine wave (resulting power range 2.5-3.5 MW). All the simulation steps are 1000 seconds. For each step sine wave period is increased in 5 second intervals, starting from 15 s and ending in 60 s. Simulation ends once these steps are completed, at 11000 seconds. Cooling is active throughout the simulation.

Table 5. Transient definitions and identification numbers. Listed form loss is applied to both heating and cooling section.

transient id	transient type	heater power (MW)	form loss
1	pulse	3	1
2	pulse	3	10
3	pulse	3	100
4	pulse	3	1000
11	flow initiation	3	1
12	flow initiation	3	10
13	flow initiation	3	100
14	flow initiation	3	1000
21	sine wave	3	1
22	sine wave	3	10
23	sine wave	3	100
24	sine wave	3	1000
31	flow initiation	0.2	1
32	flow initiation	0.2	10
33	flow initiation	0.2	100
34	flow initiation	0.2	1000

4. Simulation results

4.1 Hot water pulse in cold system

This simulation set consisted of 60 simulations, all of which started from cold 30 °C system with no circulation and active cooling. Heating was applied for 60 seconds and after that only cooling was active.

All of the cases experience a flow rate peak which is quickly dampened when driving force of the heating has ceased. For the majority of the tests, the rest of simulation is dampening oscillation between negative and positive flow. Some cases, however, experience different type of behaviour in which flow turns positive throughout the rest of the simulation. This behaviour is reviewed and explained in Chapter 4.1.1. All the cases are stabilizing and there is no unexplained behaviour. Three examples of the result graphs are show in Figures 2, 3 and 4.

Figure 1. Apros model of the circulation loop. Used expansion tank was excluded and used as a static pressure boundary. Heating section as at bottom right and cooling section is at top left. Positive circulation is counter-clockwise. Geometry variations were read into the model from SCL scripts.

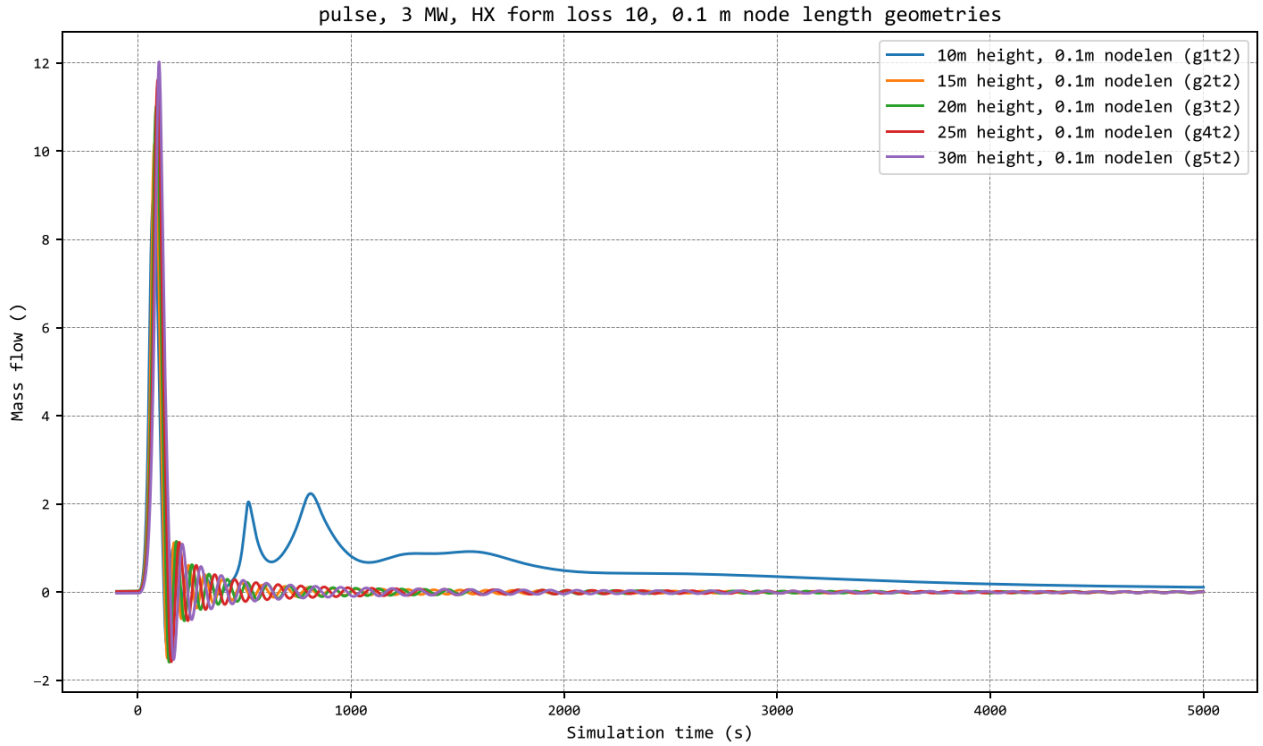

Figure 2. 3 MW, hot water pulse in cold system, form loss 10, 0.1 m target node length results.

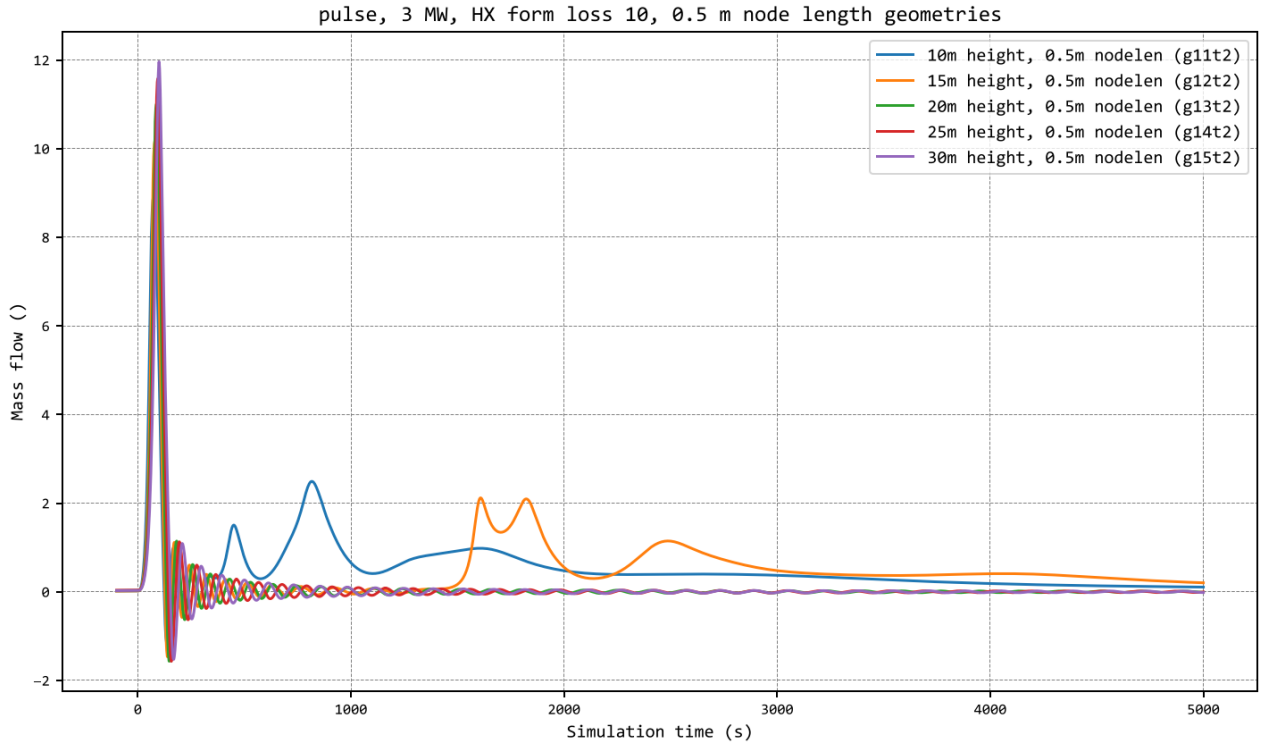

Figure 3. 3 MW, hot water pulse in cold system, form loss 10, 0.5 m target node length results.

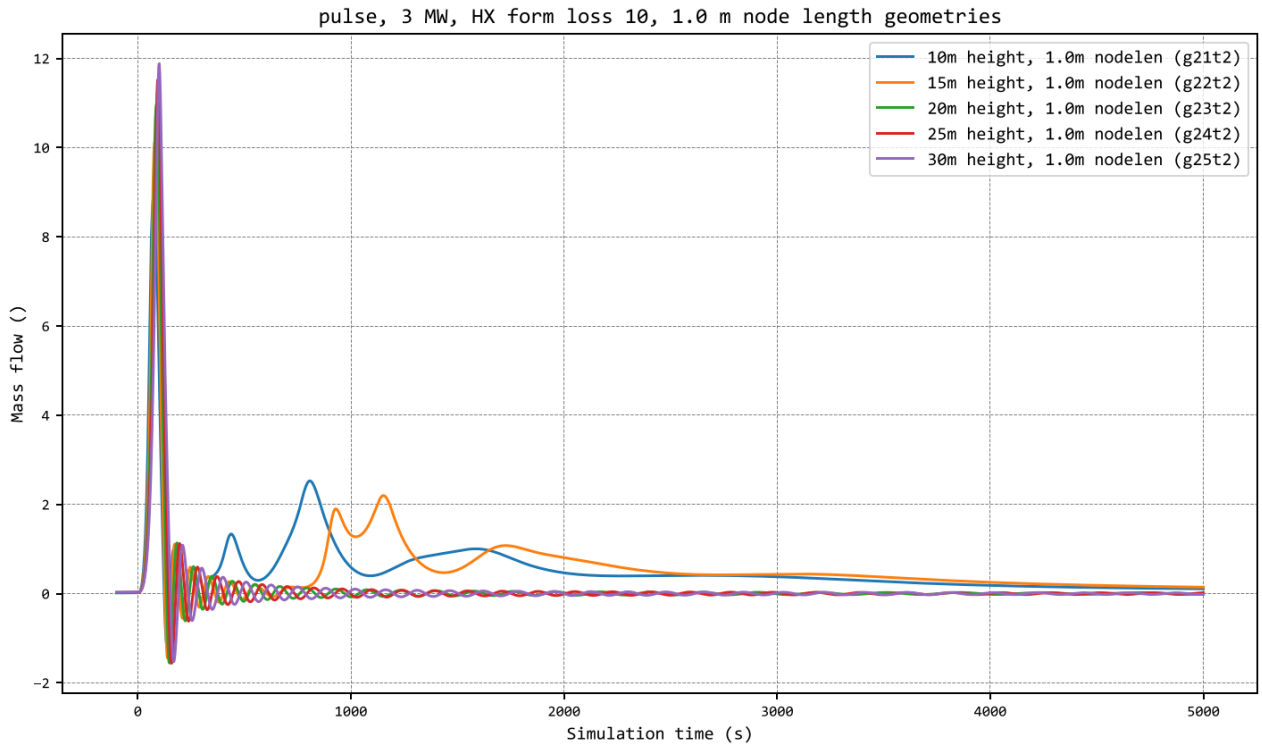

Figure 4. 3 MW, hot water pulse in cold system, form loss 10, 1.0 m target node length results.

4.1.1 Detailed review of test g12t2

Behaviour of 10 m and 15 m height geometries in hot water pulse tests was often unlike the taller counterparts. In the beginning these show the same oscillation as seen in the other tests but then mass flow suddenly goes positive and stays as such for the rest of the simulation time. One example is case g22t2, a 15-meter nodalization with 1 m target node length and form loss 10 in the heat exchangers. Since the underlaying cause didn't become evident by usual means of assessment single or few values vs. time, required data was exported to Paraview [7] for detailed study. Figures Figure 5 and Figure 6 show mass flow and velocity in the test. Reviewed sequence of events is listed on

Table 6 and Paraview visualizations are in Figures 7 and 8.

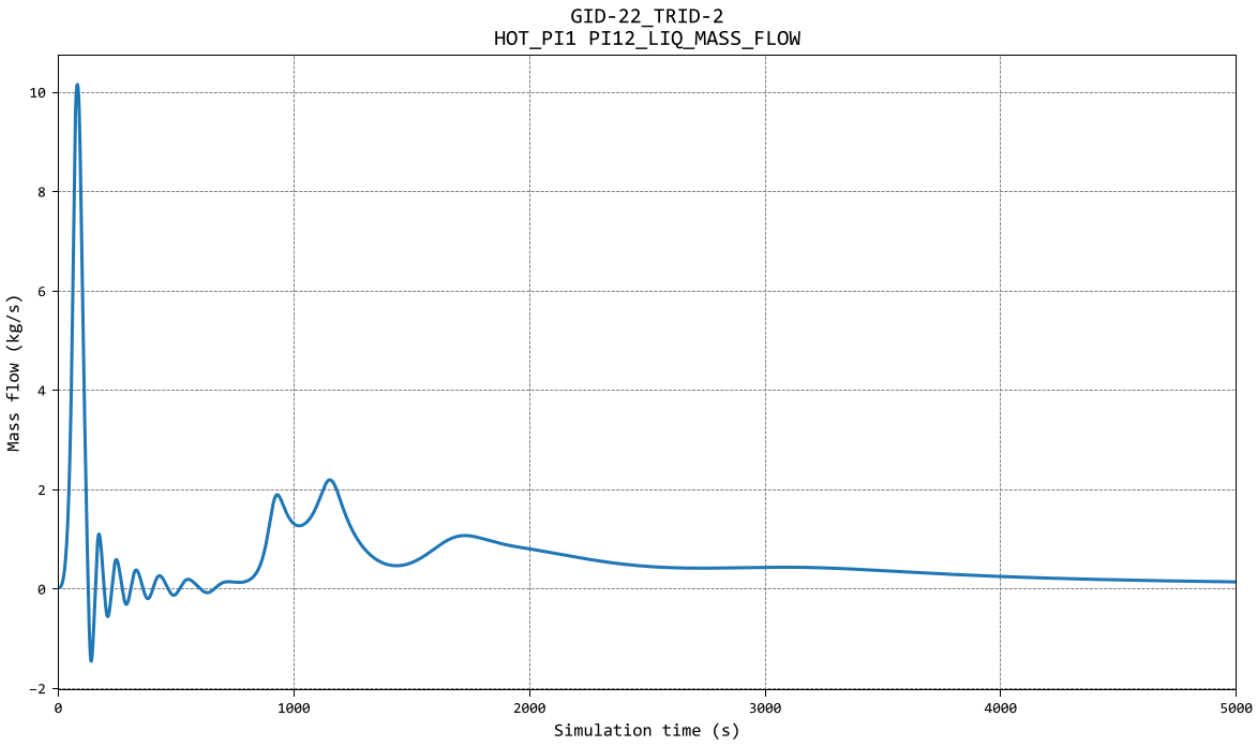

Figure 5. Unusual mass flow in case g12t2. Positive mass flow is in counter-clockwise direction.

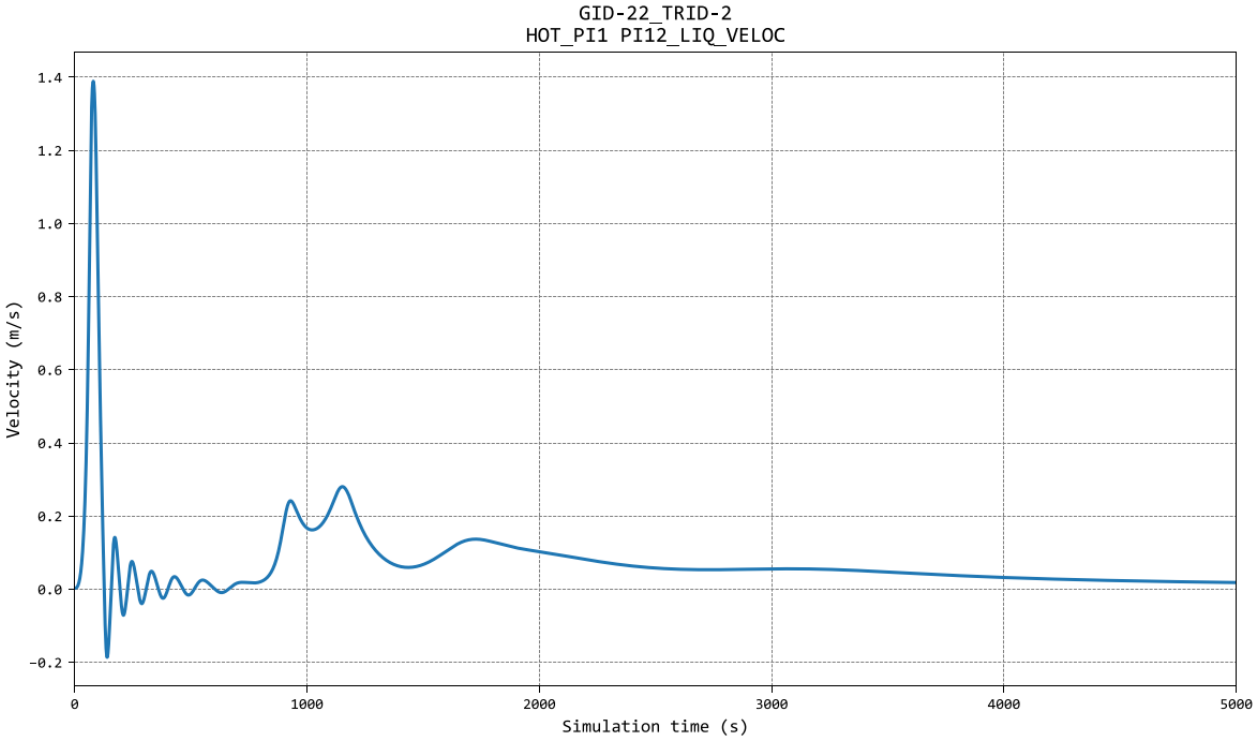

Figure 6. g22t2, hot water pulse at 3 MW, liquid velocity in riser.

Table 6. g22t2 progression (3 MW hot water pulse in cold system, 15 m geometry, 1 m target nodalization, form loss 10)

Time (s)	Description
0	System at 30 °C. Heating is started and cooling is active. Nodalization is shown. Shown(?) vertical placement is according to cell center elevations and vertically the placement is close but not exact.
60	Heating stopped. Hot water pulse is rising upwards. Cooling section remains active throughout the transient. Representation is changed to wireframe.
90	Hot water pulse has reached the cooler. Cold water has entered the heating section. This simulation time is close to maximum mass flow. Denser cold water in riser section and decreasing buoyant force are about to turn the flow negative.
110	After the maximum mass flow, flow is getting close to local minimum. Mass flow goes negative.
300	Oscillation with decreasing amplitude. Cold water in heating section prevents circulation of flow. Water is cooling section starts to cool but due to 1-dimensional flow path and no bypasses, it cannot really progress into the downcomer section. When observed frame by frame in 1 second intervals, some numerical diffusion is visible as the downcomer slowly mixes. In pipe flow this is generally unwanted but since here the 1D-geometry tries to represent an annular space with three-dimensional flow patterns, behaviour in downcomer is likely more realistic because of it. Sidenote: Majority of the other simulations seem to continue this decreasing oscillation until the end of simulation.
700	Cooler section is getting much colder than the downcomer. There is still cold water in the heating section.
900	Water in cooler section is dense enough to initiate flow. When observed frame by frame, numerical diffusion is again visible.
1100	Warmer water of downcomer has been pushed to riser. Circulation stays positive with very low velocity.
5000	Situation described at 1100 s applies all the way until end of simulation.

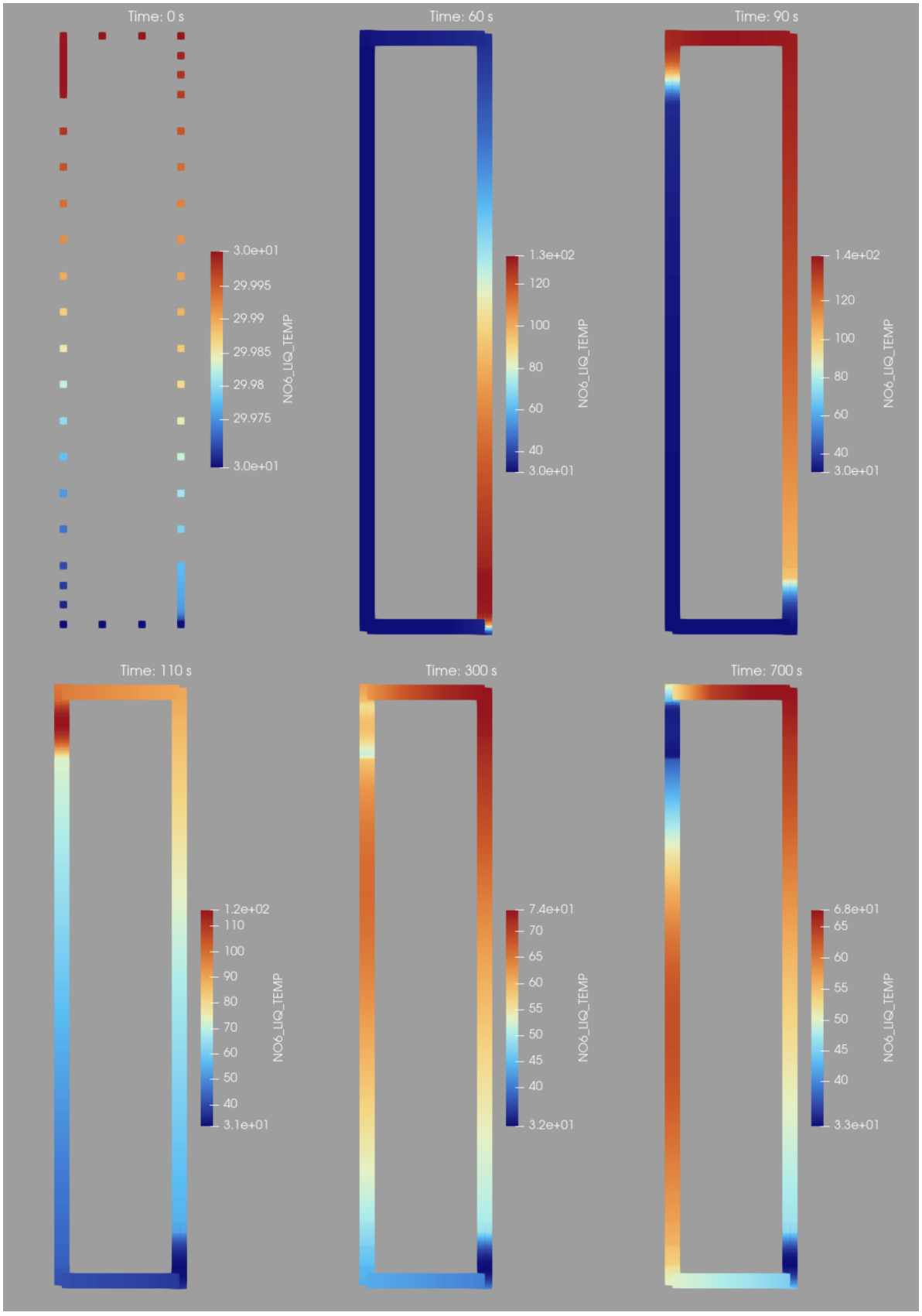

Figure 7. Case g22t2, hot water pulse at 3 MW heating power, simulation times 0-700 seconds. Each of the colour ranges are scaled to the current minimum and maximum.

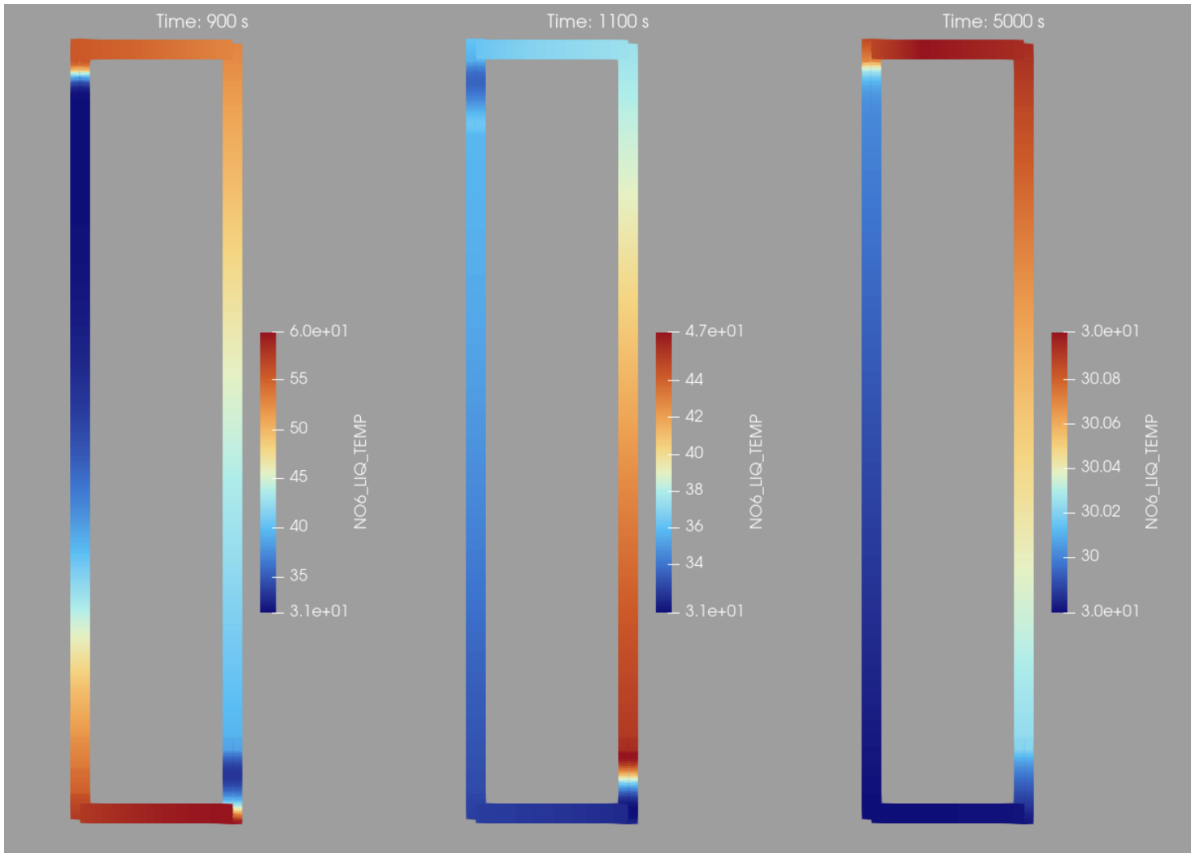

Figure 8. Case g22t2, hot water pulse, simulation times 900-5000 seconds.

The cause of different and therefore seemingly odd behaviour proved not to be an error of the code but a side effect of the super-simple nodalization. Closer examination revealed nothing unphysical that is not explained by the used nodalization and numerical diffusion. The only negative aspect is that this behaviour couldn't be explained using the built-in tools. Apros calculation level visualization can provide a somewhat similar view, but a better time management was the key element in understanding event progression.

4.2 Flow initiation

This simulation set consisted of 60 simulations for 3 MW power and another 60 simulations for 200 kW power, all of which started from 30 °C system. Heating and cooling were active through the simulation.

The results show that higher the geometry, bigger the oscillations before system finds a steady-state. Majority of the startup tests show steadily dampening oscillation like shown in Figure 9. All the 3 MW cases reached steady-state by 800 s.

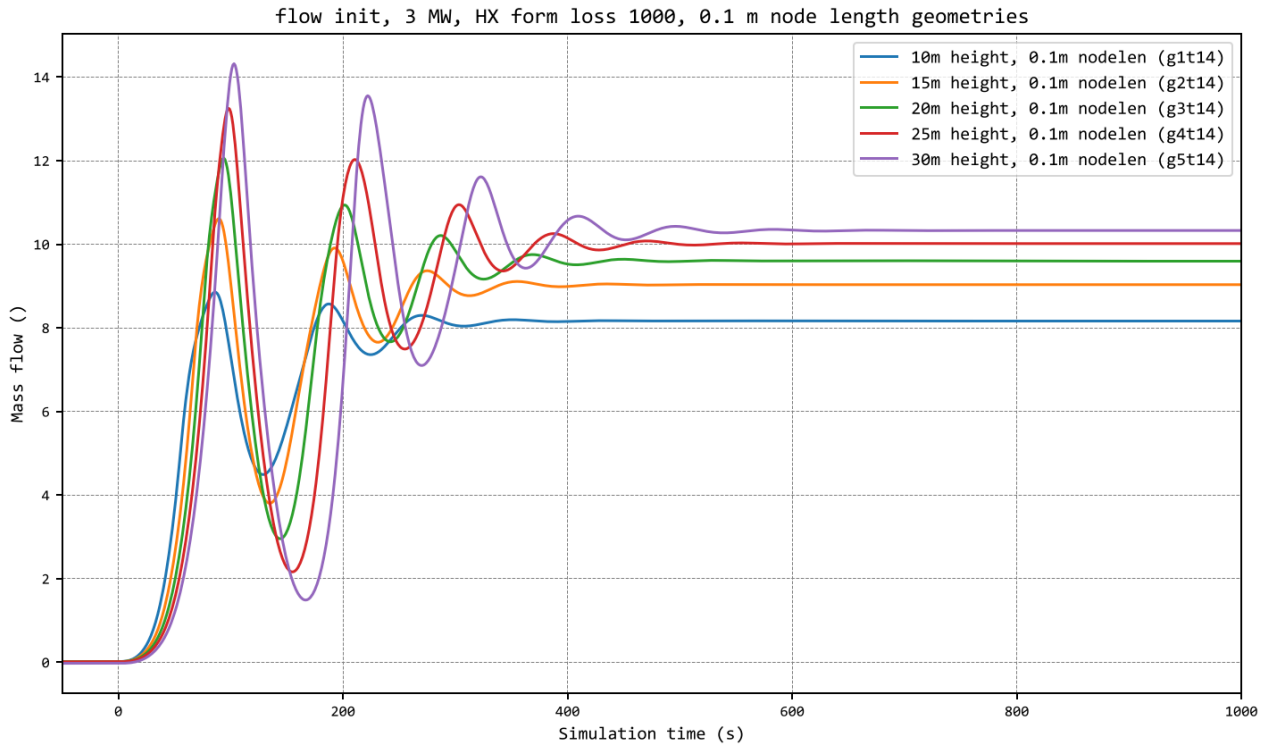

Figure 9. 3 MW flow initiation, form loss 1000, 0.1 m target node length. Effect of loop height on stabilization and final mass flow.

Figure 10 shows the effect of nodalization on system behaviour. Denser nodalization leads to slightly larger amplitude when the system is finding steady-state but all the configurations eventually find the same steady-state. It can be speculated that the small differences are at least partially caused by numerical diffusion and how it affects temperature fronts.

All the 3 MW flow initiation results are collected in Appendix 1.

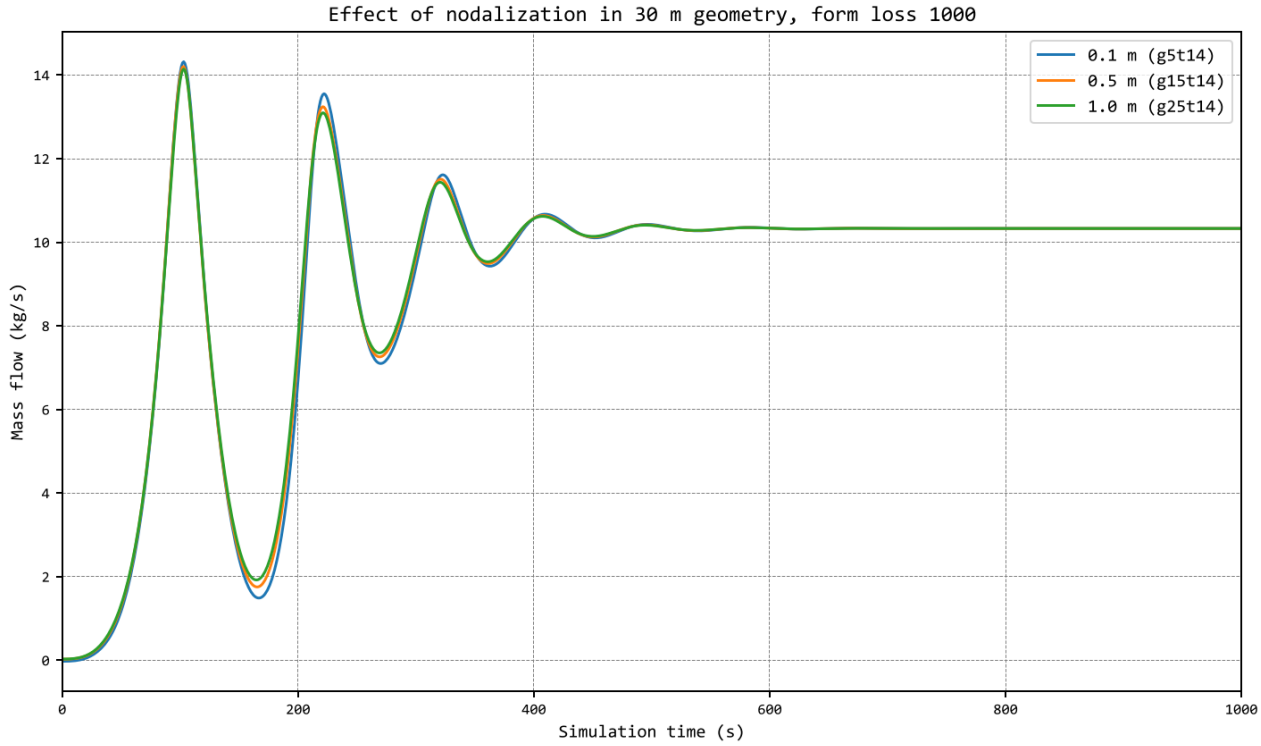

Figure 10. 3 MW flow initiation, effect of nodalization length in 30 m geometry with highest form loss (1000).

As expected, flow losses have dampening effect on oscillations. This is shown in Figure 11.

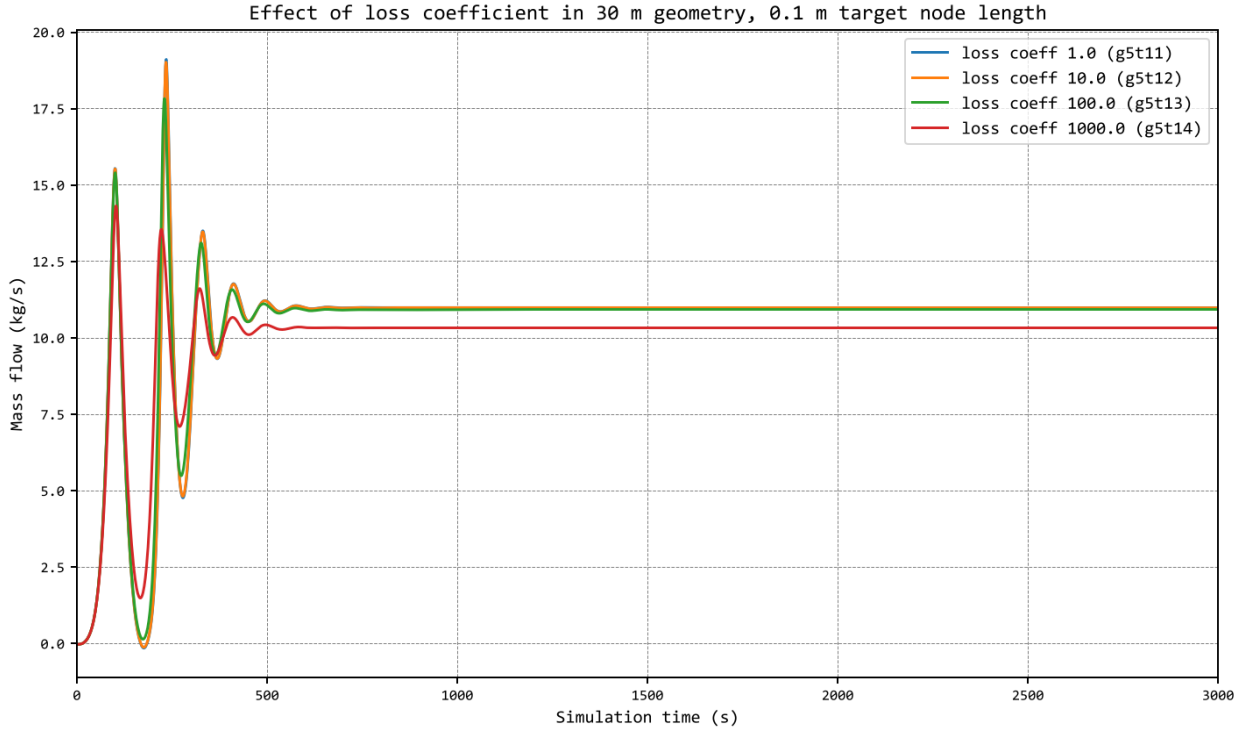

Figure 11. 3 MW flow initiation, 30 m height, 0.1 target node length. Effect of flow losses on stabilization.

Lower driving force from heating in the 200 kW flow initiation tests leads to slower system response and finding a final steady-state takes considerably longer. Comparison to 3 MW is shown in Figure 12. All the 200 kW tests show steadily dampening oscillation. An example is shown in Figure 13

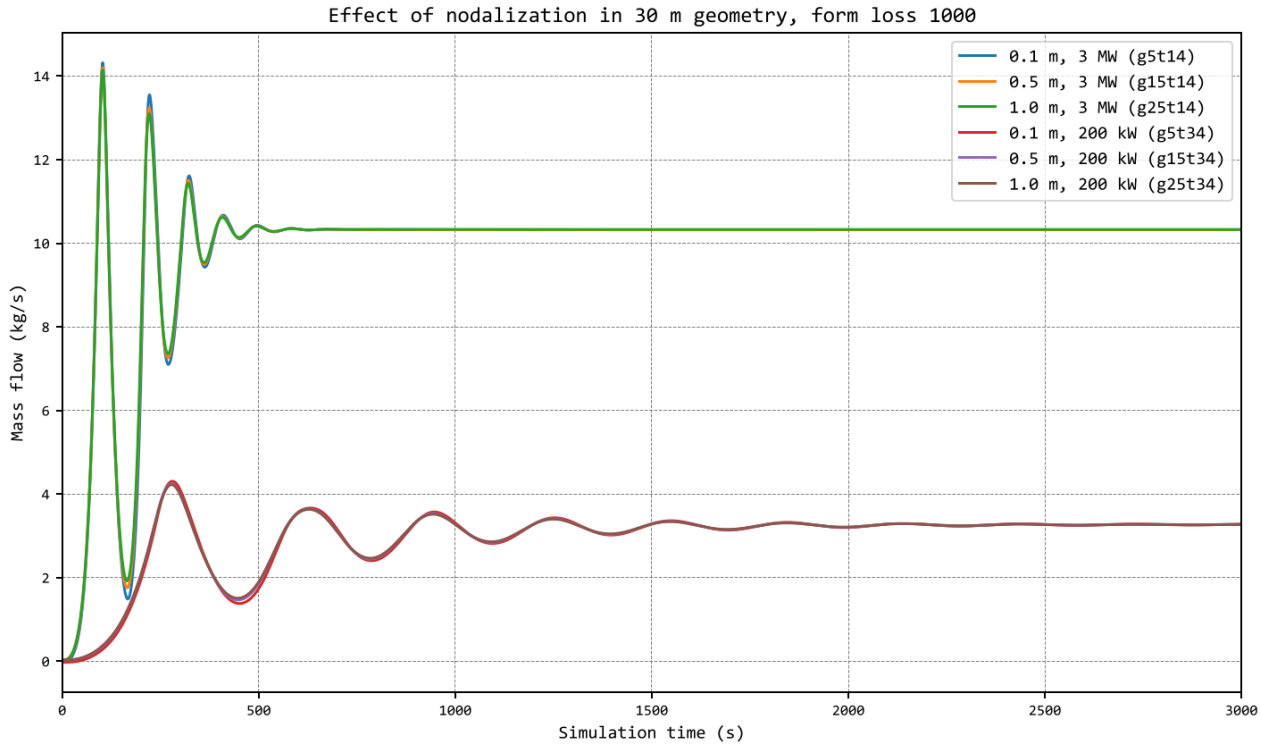

Figure 12. Comparison of selected 3 MW and 200 kW flow initiation tests. The compared three cases are otherwise identical except for heating power.

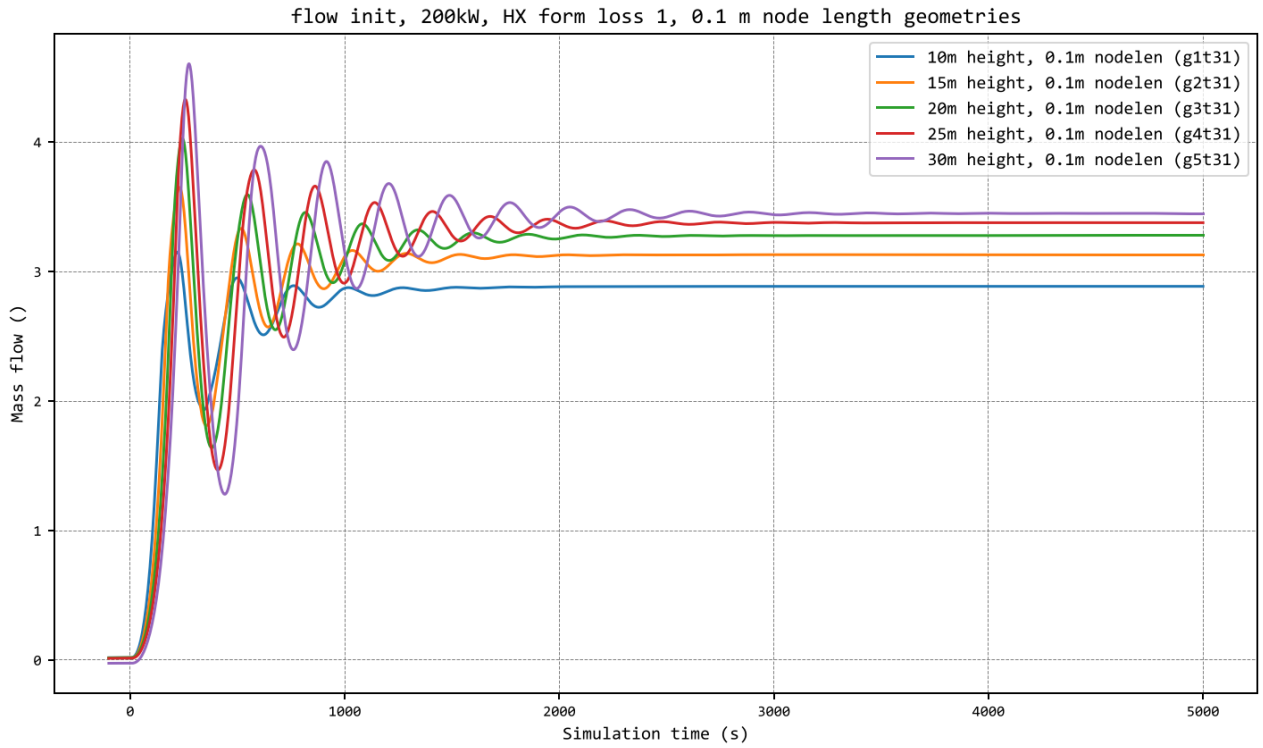

Figure 13. 200 kW flow initiation, form loss 1, 0.1 node target length.

Interestingly in some 25 m and 30 m geometries the second flow maximum is higher than the first one. This short-term instability is rather interesting, but the sequence of events couldn't be reviewed in Paraview because the inspection workflow[2], used in Chapters 4.1.1 and 4.2.1, was completed only for single geometry-nodalization combination. However, since the flow is driven by having colder water in downcomer and warmer water in riser, it can be speculated that after first maximum the system reaches a state where downcomer and relatively warm and riser is relatively cold. When the water in heating section heats up, flow increases and at the same time the warmer water enters the heating section, enhancing the driving force. By third cycle this behaviour is over and the system is stabilizing.

This behaviour is most prominent with 30 m nodalization with 0.1 target nodal length and lowest resistance in the circuit (Figure 14). With the highest flow resistance (loss coefficient 1000) it is no longer present (Figure 15). The cases where second maximum is higher than the first are collected in Table 7. Based on this limited set, the behaviour seems to be more prominent in tighter nodalizations and higher flow resistance leads to more stable system. It's likely that these cases have the correct geometry, heating power and flow loss combination to enable this behaviour. Nodalization having effect may relate to numerical diffusion (with short nodes hot or cold water front likely stays more intact).

[2] Detailed inspection workflow was completed only for 15 m height geometry using 1 m target nodalization length. Exporting data from Apros to Paraview required separated simulations for reviewed cases, using separate dataset definitions. Additionally, the process required manual steps like mapping x, y coordinates as input for conversion script.

This behaviour can only be seen in 3 MW simulations and 200 kW flow initiations all show decreasing amplitude.

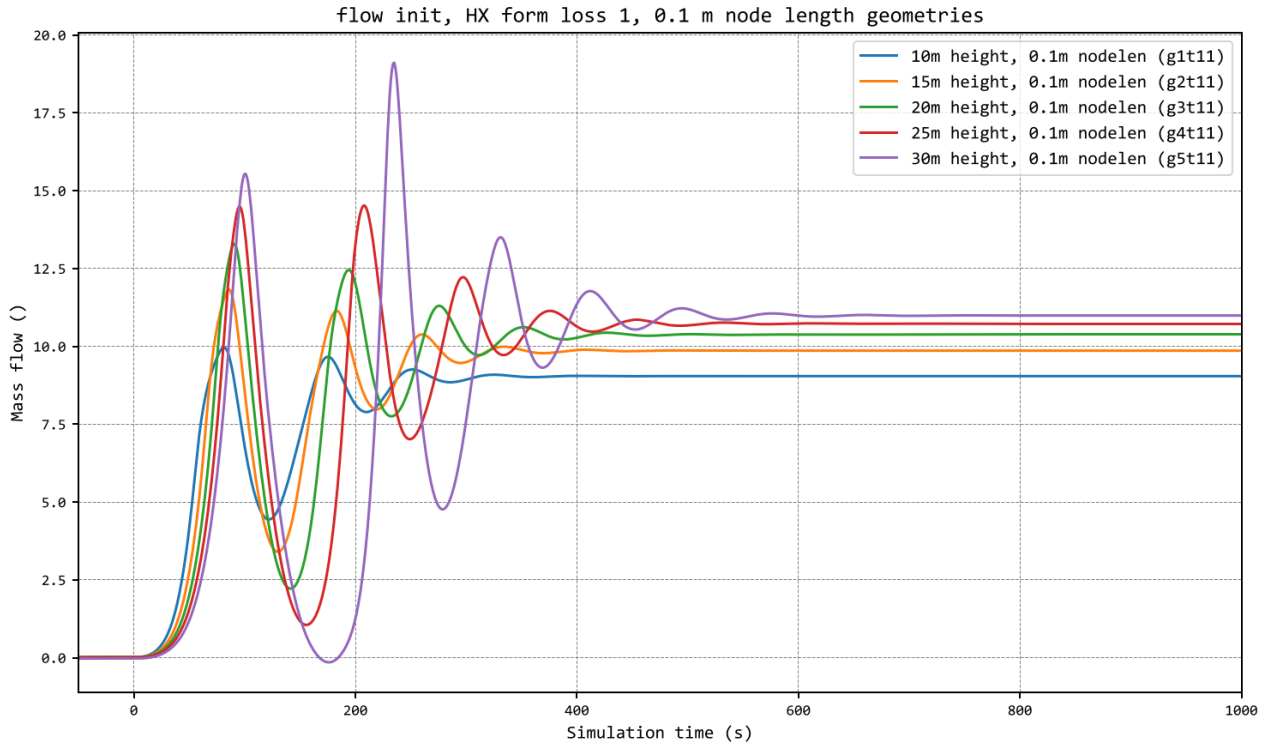

Figure 14. 3 MW flow initiations cases with 0.1 target calculation node length and form loss 1 in the heat exchangers. Case g5t11 is the most prominent example of second flow maximum exceeding the initial one.

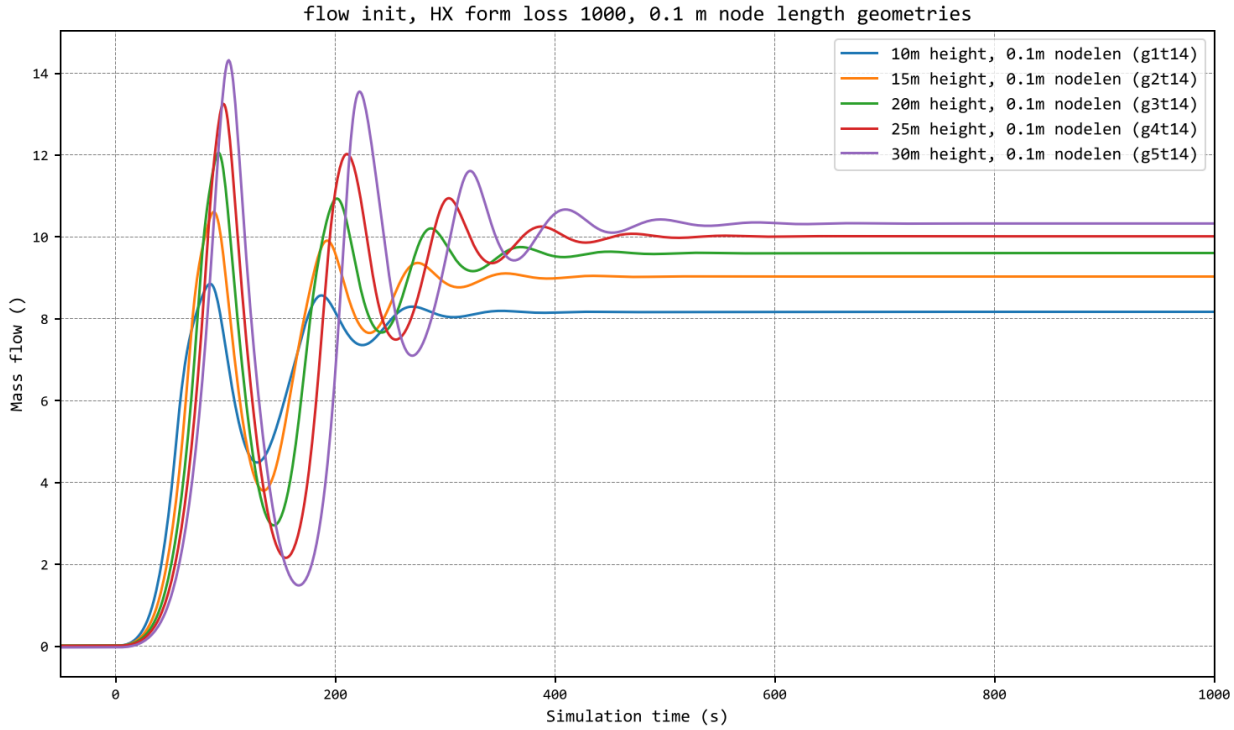

Figure 15. 3 MW flow initiations cases with 0.1 target calculation node length and form loss 1000 in the heat exchangers. These cases are otherwise identical to Figure 14 except for higher flow resistance.

Table 7. Flow initiations cases in which the second flow maximum exceeds the initial one. In all cases the system is stabilizing by third local maximum.

id	transient type	power (MW)	height (m)	node target length (m)	form loss	max mass flow (kg/s)	steady-state mass flow (kg/s)	overshoot (%)	steady-state liquid velocity (m/s)
g4t11	flow initiation	3	25	0.1	1	14.525	10.732	35.3	1.526
g4t12	flow initiation	3	25	0.1	10	14.486	10.724	35.1	1.526
g5t11	flow initiation	3	30	0.1	1	19.111	10.992	73.9	1.561
g5t12	flow initiation	3	30	0.1	10	19.020	10.985	73.1	1.560
g5t13	flow initiation	3	30	0.1	100	17.828	10.918	63.3	1.551
g15t11	flow initiation	3	30	0.5	1	16.912	10.992	53.9	1.561
g15t12	flow initiation	3	30	0.5	10	16.840	10.985	53.3	1.560
g15t13	flow initiation	3	30	0.5	100	16.229	10.918	48.6	1.551
g25t11	flow initiation	3	30	1	1	16.155	10.992	47.0	1.561
g25t12	flow initiation	3	30	1	10	16.107	10.985	46.6	1.560
g25t13	flow initiation	3	30	1	100	15.654	10.918	43.4	1.551

4.2.1 Detailed review of test g22t12

As an example of flow startup simulation, case g22t12, was chosen for detailed review. This case uses the same nodalization and options as previously shown g22t2, except for being of flow initiation type (in which the heating is not stopped at 60 s).

Riser mass flow and velocity are show in Figures Figure 16 and Figure 17. Transient progression is reviewed in Table 8. Simulation times beyond 185 s are not shown since wide temperature range hides most of the details. The rest of simulation remains visually very similar to the last shown simulation time.

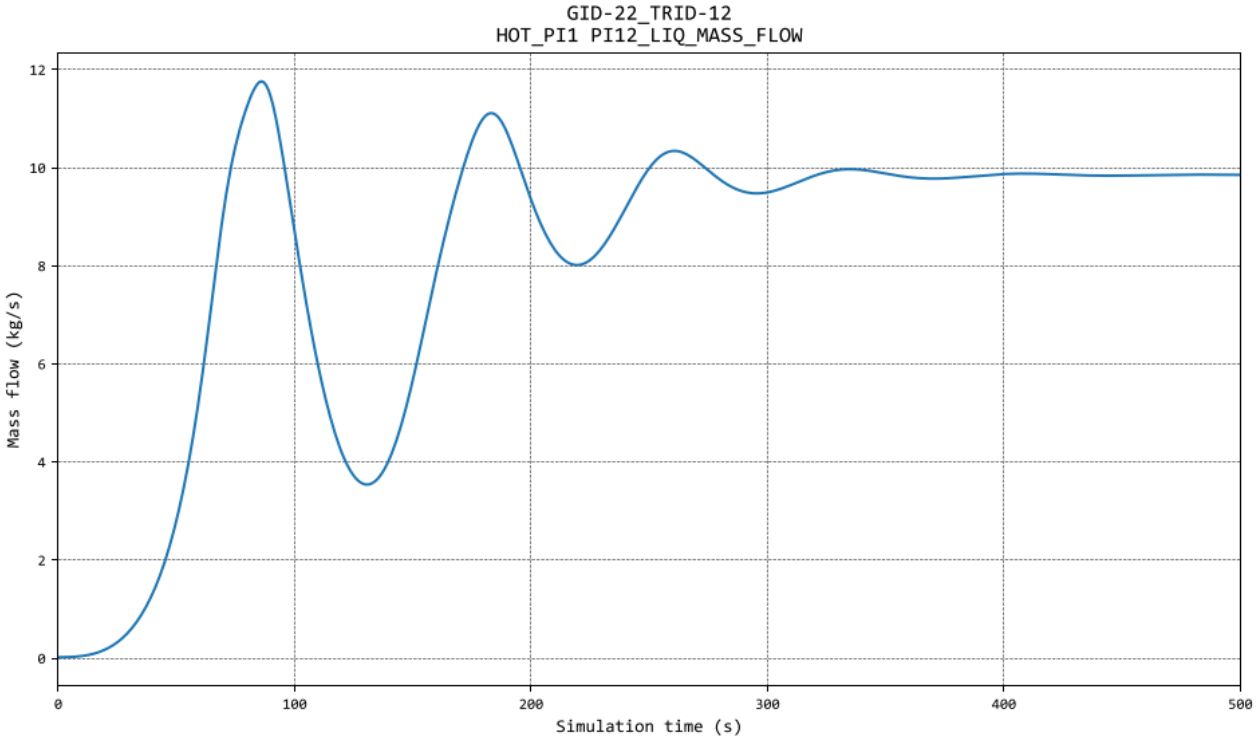

Figure 16. g22t12, flow initiation at 3 MW, form loss 10, liquid mass flow.

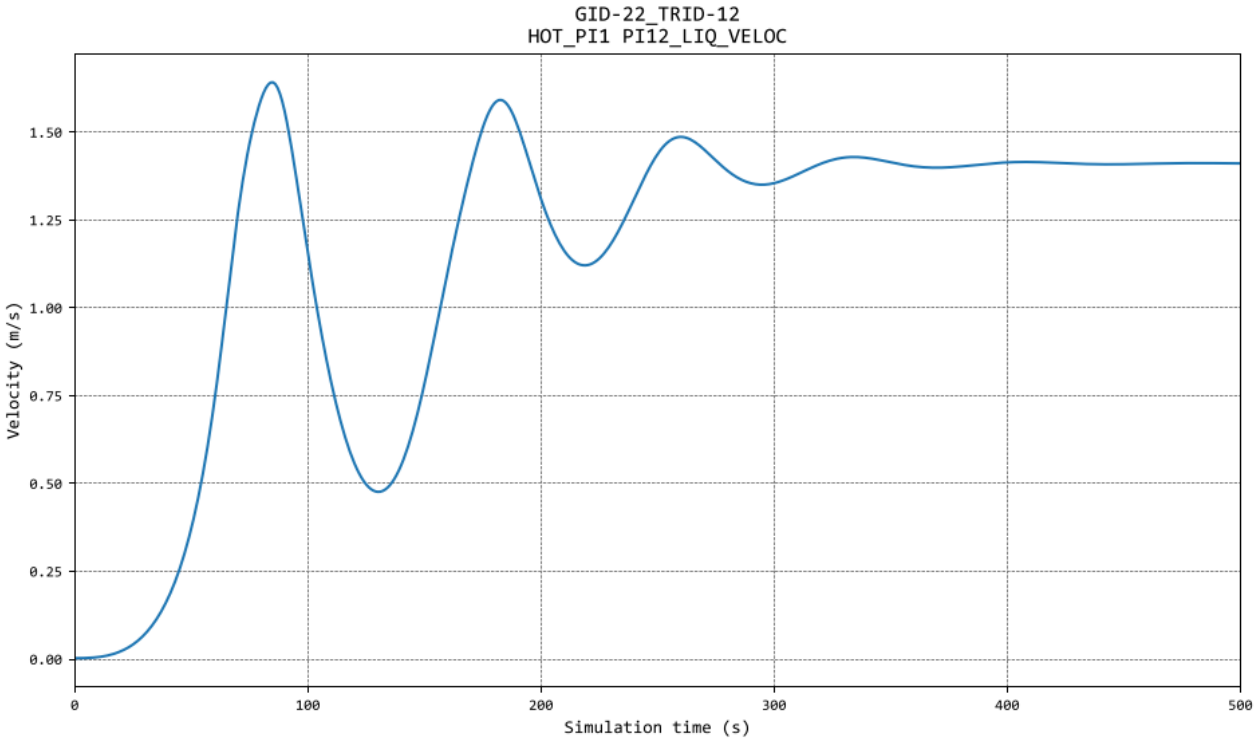

Figure 17. g2212, flow initiation at 3 MW, form loss 10, liquid velocity in riser.

Table 8. g22t12 progression (3 MW flow initiation, 15 m geometry, 1 m target nodalization, form loss 10)

Time (s)	Description
0	System is at 30 °C. Heating is started and cooling is active. Nodalization is shown. Shown vertical placement is according to cell center elevations and vertically the placement is close but not exact.
60	Hot water pulse is rising upwards in the riser
90	Near flow maximum. Hot water has reached the cooler. Downcomer is cold and riser is hot.
110	Closing to local flow minimum. Downcomer is now warmer and cold water has pushed into heater.
150	Flowrate has been slow and heater has had time to heat up water. Flowrate is rising.
185	Second flow maximum. Hot water has risen up and at the same time colder water has pushed into the heater. Flowrate is about to drop, which will give heater time to heat up the water and another cycle will start. The rest of the simulation looks visually similar to this state and is not shown.

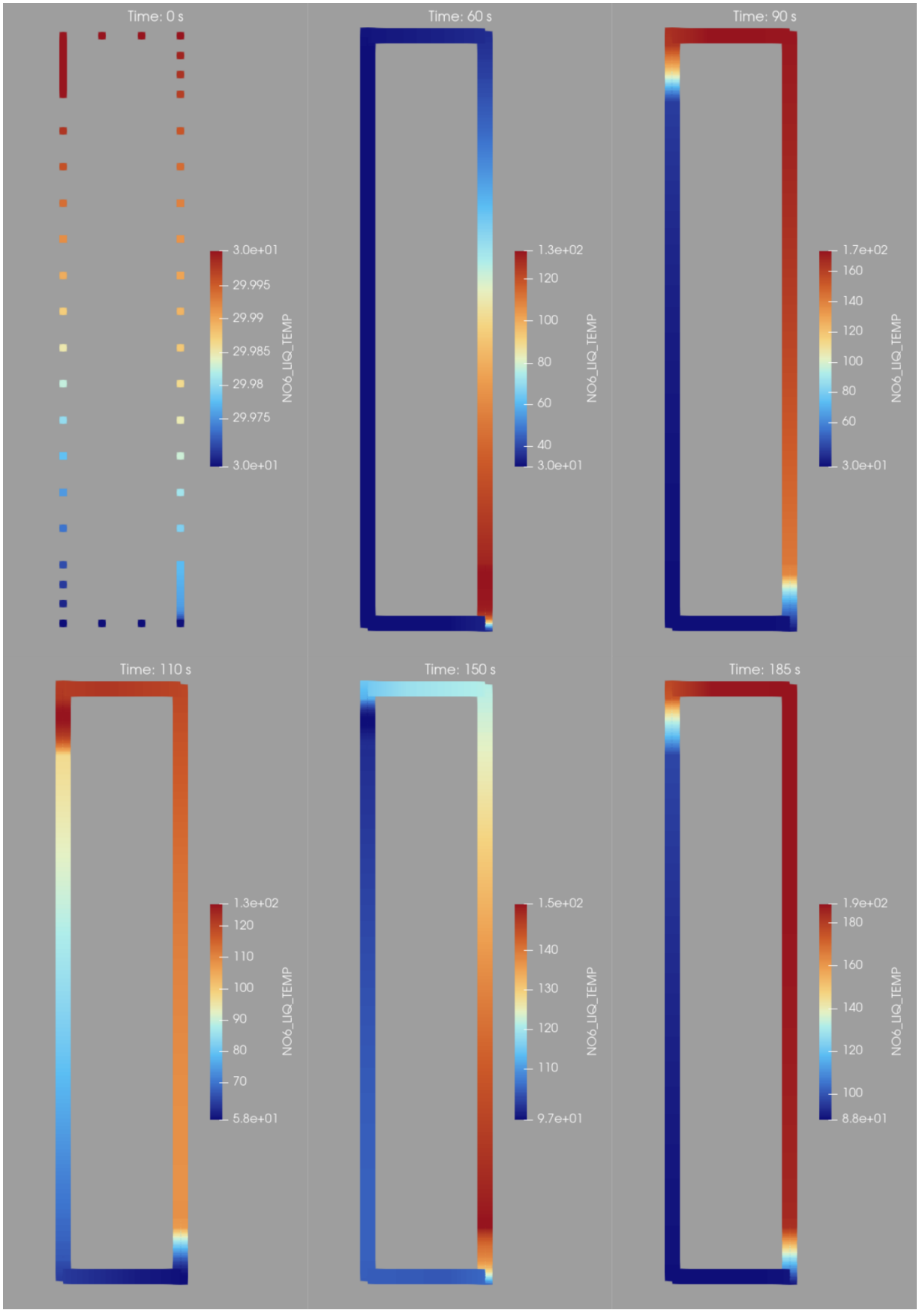

Figure 18. Case g22t12, flow initiation at 3 MW, simulation times 0-185 s.

4.3 Sine wave power

In sine wave tests the boundary power was formed as sine wave, ranging from 2.5 MW to 3.5 MW. 60 simulations were made which each consisted of 11 parts of varying sine wave period. Total number of tested simulation states was 660.

The simulations show that changing sine wave period causes a temporary disturbance[3] but after few periods, in all the cases, the system shows oscillation with steady amplitude. Longer the boundary power period, the more the system has time to reach a state that suits that particular power level. With short periods mass flow is always close to the 3 MW circulation rate. Flow losses dampen the oscillations. Two examples of the test series are shown in Figures 19 and 20. The rest of the test series is very similar and is not shown. The system was found to be stable in all the tested combinations.

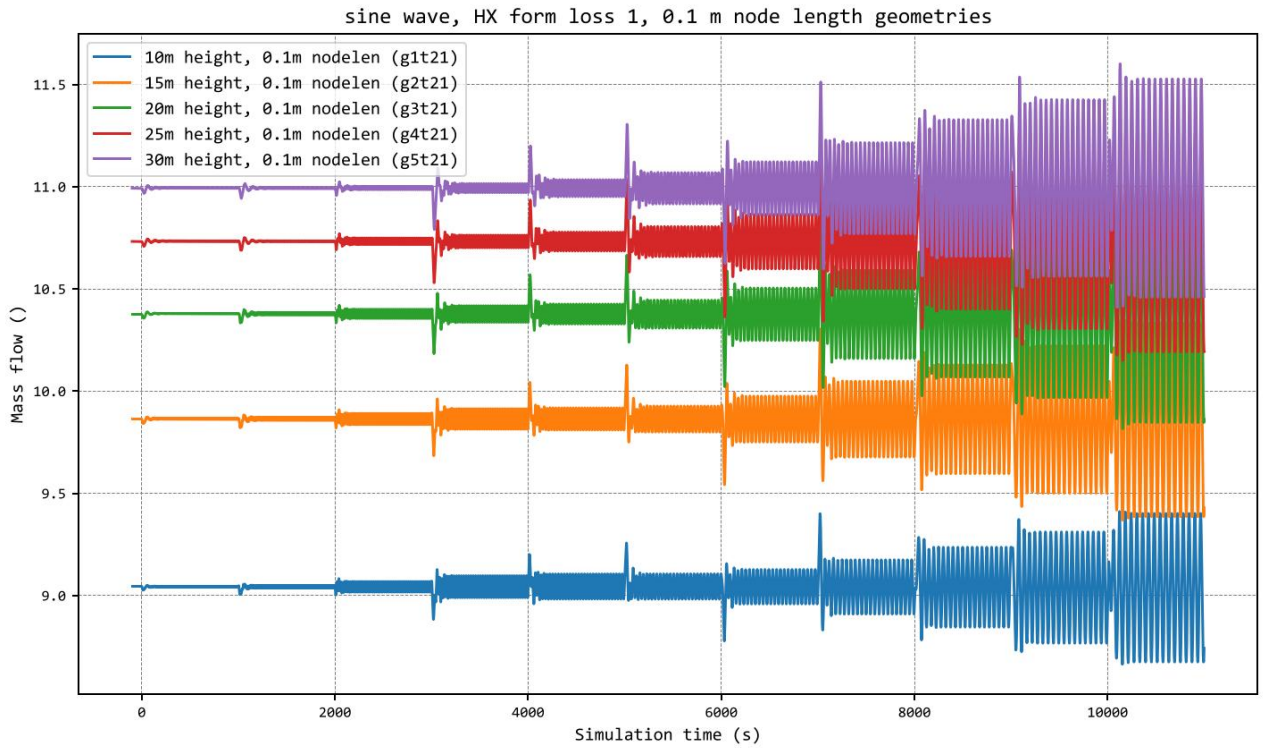

Figure 19. 3 MW ± 0.5 MW sine wave boundary power, form loss 1, 0.1 node target length.

[3] This is party cause by the modelled sine wave generator which doesn't continue from the previous power level.

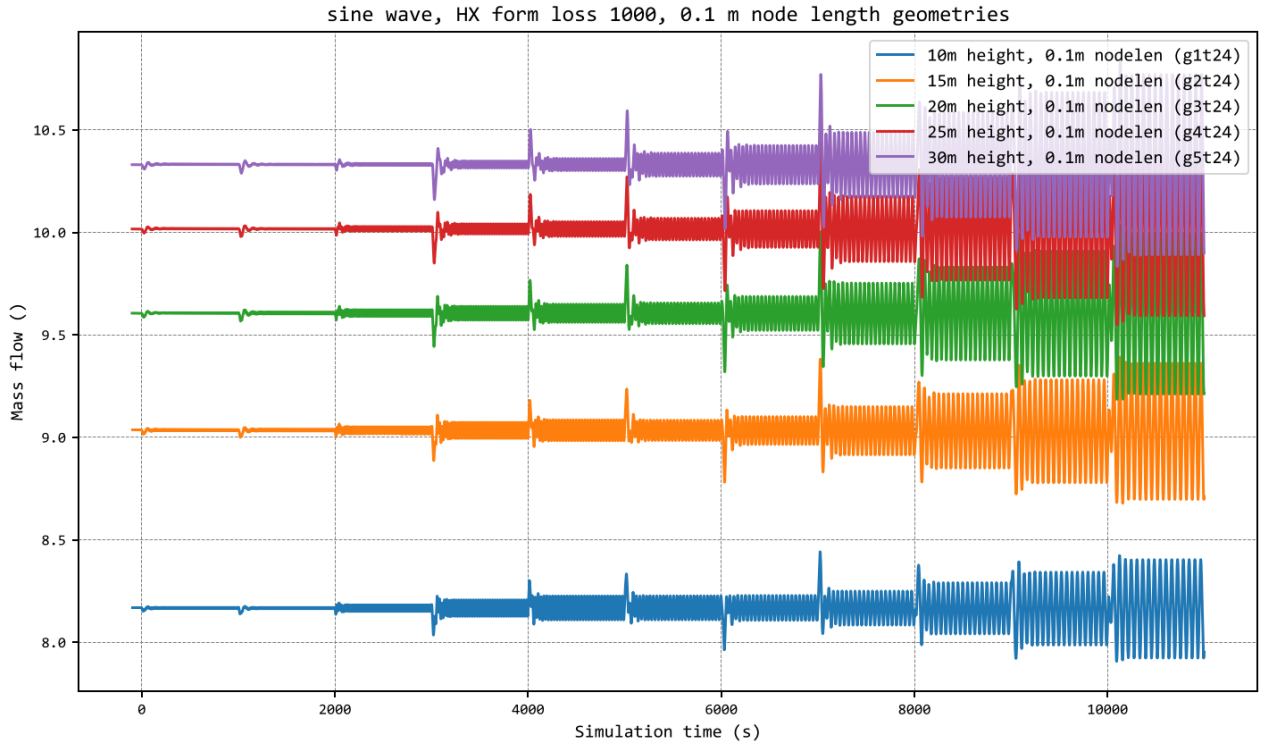

Figure 20. 3 MW ± 0.5 MW sine wave boundary power, form loss 1000, 0.1 m node target length.

5. Discussion

The simulations demonstrated how even a simple geometry can provide interesting insight into flow solution when inspected at required level. The modelled loop was kept simple by design to allow use of multiple geometries and nodalizations. The result was a system which contained no bypass or turned flow possibilities for either heater section (e.g. core) or cooler section (e.g. steam generator). Single dimensional loop flow path led to exaggeration of oscillations and in some tests, flow behaviour that was completely different from other cases. All findings, however, were explainable by the nodalization and nature of the flow solution.

The temporary second-maximum instability seen in some of the flow initiation cases could be, to some extent, a real phenomenon in some SMR designs. However, the modelled test setup was built to increase the likelihood of instabilities and therefore it exaggerates the phenomenon. If the setup would have had pipe walls, the system would have been more stable. If the instability is present in some designs, it likely has limited safety meaning, but it will first need to be identified and then accounted in the control system logic and startup procedures.

The findings emphasized the importance of modeller understanding the task at hand. Oversimplifying flow paths can lead to effects that are unphysical. The solution, however, is not to make everything in model more complex – modelling complex three-dimensional flow patterns is a realm of CFD, and 1D-modelling is by necessity a simplification. The question lies where these simplifications are made and how they affect the simulation result. In interpreting results, Apros would benefit from visualization system in which colour gradients can be used to visualize attribute values and time management would allow scrolling simulation timeline back and forth. This would allow a workflow that enables efficient identification of problems, corrections to the model and greatly improve the understanding of the model.

6. Summary

Apros natural circulation has been tested in rectangular closed loop geometry using 5 different loop heights, 3 different nodalization, 4 different loop flow resistances and using three different test types. In total 240 single phase simulations were performed, of which tested a total of 840 states. All of the tested cases proved ultimately stable.

The reviewed simulation set revealed nothing suspicious in Apros' capability in modelling natural circulation of SMR designs. Unrealistic behaviour seen in some of the tests can be attributed to too simple nodalization. The simulations highlighted the potential for user error when trying to over-simplify geometries that encounter three-dimensional flow patterns, especially at very low powers.

References

[1] Y. Farawila and M. Presson, 'NuScale Topical Report Evaluation Methodology for Stability Analysis of the NuScale Power Module', Jun. 10, 2019. [Online]. Available: https://www.nrc.gov/docs/ML1919/ML19192A166.pdf

[2] D. S. Pilkhwal, W. Ambrosini, N. Forgione, P. K. Vijayan, D. Saha, and J. C. Ferreri, 'Analysis of the unstable behaviour of a single-phase natural circulation loop with one-dimensional and computational fluid-dynamic models', *Ann. Nucl. Energy*, vol. 34, no. 5, pp. 339–355, May 2007, doi: 10.1016/j.anucene.2007.01.012.

[3] P. K. Vijayan *et al.*, 'Investigations on the Effect of Heater and Cooler orientation on the Steady State, Transient and Stability Behaviour of Single-Phase Natural Circulation in a Rectangular Loop', 2001.

[4] P. K. Vijayan, A. K. Nayak, D. Saha, and M. R. Gartia, 'Effect of Loop Diameter on the Steady State and Stability Behaviour of Single-Phase and Two-Phase Natural Circulation Loops', *Sci. Technol. Nucl. Install.*, vol. 2008, pp. 1–17, 2008, doi: 10.1155/2008/672704.

[5] F. D'Auria, A. D. Nevo, and N. Muellner, 'INSIGHTS INTO NATURAL CIRCULATION STABILITY', 2010.

[6] Jose Reyes, 'Natural Circulation in Water Cooled Nuclear Power Plants Phenomena, models, and methodology for system reliability assessments', DOE/ID/14550, 836896, Feb. 2005. doi: 10.2172/836896.

[7] 'Paraview homepage'. [Online]. Available: https://www.paraview.org/

Appendix 1. 3 MW flow initiation results

3 MW flow initiation results are collected in Tables 9-13. Steady-state mass flow and liquid velocity are recorded from riser at the end of simulation. Overshoot is calculated from maximum mass flow and steady-state mass flow.

Table 9. 3 MW flow initiations in 10 m geometries

id	transient type	power (MW)	height (m)	node target length (m)	K-loss	max mass flow (kg/s)	steady-state mass flow (kg/s)	overshoot (%)	steady-state liquid velocity (m/s)
g1t11	flow initiation	3	10	0.1	1	9.969	9.045	10.2	1.305
g1t12	flow initiation	3	10	0.1	10	9.956	9.035	10.2	1.304
g1t13	flow initiation	3	10	0.1	100	9.832	8.939	10.0	1.291
g1t14	flow initiation	3	10	0.1	1000	8.856	8.169	8.4	1.191
g11t11	flow initiation	3	10	0.5	1	9.949	9.045	10.0	1.305
g11t12	flow initiation	3	10	0.5	10	9.936	9.035	10.0	1.304
g11t13	flow initiation	3	10	0.5	100	9.816	8.939	9.8	1.291
g11t14	flow initiation	3	10	0.5	1000	8.842	8.168	8.2	1.191
g21t11	flow initiation	3	10	1	1	9.938	9.045	9.9	1.305
g21t12	flow initiation	3	10	1	10	9.925	9.035	9.9	1.304
g21t13	flow initiation	3	10	1	100	9.805	8.939	9.7	1.291
g21t14	flow initiation	3	10	1	1000	8.834	8.168	8.1	1.191

Table 10. 3 MW flow initiations in 15 m geometries.

id	transient type	power (MW)	height (m)	node target length (m)	K-loss	max mass flow (kg/s)	steady-state mass flow (kg/s)	overshoot (%)	steady-state liquid velocity (m/s)
g2t11	flow initiation	3	15	0.1	1	11.828	9.864	19.9	1.412
g2t12	flow initiation	3	15	0.1	10	11.815	9.855	19.9	1.411
g2t13	flow initiation	3	15	0.1	100	11.679	9.767	19.6	1.400
g2t14	flow initiation	3	15	0.1	1000	10.612	9.035	17.5	1.304
g12t11	flow initiation	3	15	0.5	1	11.802	9.864	19.7	1.412
g12t12	flow initiation	3	15	0.5	10	11.789	9.855	19.6	1.411
g12t13	flow initiation	3	15	0.5	100	11.656	9.767	19.3	1.400
g12t14	flow initiation	3	15	0.5	1000	10.593	9.034	17.3	1.304
g22t11	flow initiation	3	15	1	1	11.777	9.864	19.4	1.412
g22t12	flow initiation	3	15	1	10	11.764	9.855	19.4	1.411
g22t13	flow initiation	3	15	1	100	11.630	9.767	19.1	1.400
g22t14	flow initiation	3	15	1	1000	10.573	9.034	17.0	1.304

Table 11. 3 MW flow initiations in 20 m geometries.

id	transient type	power (MW)	height (m)	node target length (m)	K-loss	max mass flow (kg/s)	steady-state mass flow (kg/s)	overshoot (%)	steady-state liquid velocity (m/s)
g3t11	flow initiation	3	20	0.1	1	13.289	10.378	28.1	1.480
g3t12	flow initiation	3	20	0.1	10	13.276	10.369	28.0	1.479
g3t13	flow initiation	3	20	0.1	100	13.142	10.289	27.7	1.468
g3t14	flow initiation	3	20	0.1	1000	12.061	9.606	25.6	1.379
g13t11	flow initiation	3	20	0.5	1	13.245	10.377	27.6	1.480
g13t12	flow initiation	3	20	0.5	10	13.232	10.369	27.6	1.479
g13t13	flow initiation	3	20	0.5	100	13.103	10.289	27.3	1.468
g13t14	flow initiation	3	20	0.5	1000	12.014	9.606	25.1	1.379
g23t11	flow initiation	3	20	1	1	13.216	10.377	27.4	1.480
g23t12	flow initiation	3	20	1	10	13.203	10.369	27.3	1.479
g23t13	flow initiation	3	20	1	100	13.072	10.289	27.1	1.468
g23t14	flow initiation	3	20	1	1000	11.987	9.606	24.8	1.379

Table 12. 3 MW flow initiations in 25 m geometries

id	transient type	power (MW)	height (m)	node target length (m)	K-loss	max mass flow (kg/s)	steady-state mass flow (kg/s)	overshoot (%)	steady-state liquid velocity (m/s)
g4t11	flow initiation	3	25	0.1	1	14.525	10.732	35.3	1.526
g4t12	flow initiation	3	25	0.1	10	14.486	10.724	35.1	1.526
g4t13	flow initiation	3	25	0.1	100	14.351	10.651	34.7	1.516
g4t14	flow initiation	3	25	0.1	1000	13.254	10.017	32.3	1.432
g14t11	flow initiation	3	25	0.5	1	14.419	10.732	34.4	1.526
g14t12	flow initiation	3	25	0.5	10	14.405	10.724	34.3	1.526
g14t13	flow initiation	3	25	0.5	100	14.283	10.651	34.1	1.516
g14t14	flow initiation	3	25	0.5	1000	13.190	10.017	31.7	1.432
g24t11	flow initiation	3	25	1	1	14.387	10.732	34.1	1.526
g24t12	flow initiation	3	25	1	10	14.375	10.724	34.0	1.525
g24t13	flow initiation	3	25	1	100	14.248	10.651	33.8	1.516
g24t14	flow initiation	3	25	1	1000	13.157	10.016	31.4	1.432

Table 13. 3 MW flow initiations in 30 m geometries.

id	transient type	power (MW)	height (m)	node target length (m)	K-loss	max mass flow (kg/s)	steady-state mass flow (kg/s)	overshoot (%)	steady-state liquid velocity (m/s)
g5t11	flow initiation	3	30	0.1	1	19.111	10.992	73.9	1.561
g5t12	flow initiation	3	30	0.1	10	19.020	10.985	73.1	1.560
g5t13	flow initiation	3	30	0.1	100	17.828	10.918	63.3	1.551
g5t14	flow initiation	3	30	0.1	1000	14.320	10.330	38.6	1.474
g15t11	flow initiation	3	30	0.5	1	16.912	10.992	53.9	1.561
g15t12	flow initiation	3	30	0.5	10	16.840	10.985	53.3	1.560
g15t13	flow initiation	3	30	0.5	100	16.229	10.918	48.6	1.551
g15t14	flow initiation	3	30	0.5	1000	14.206	10.330	37.5	1.474
g25t11	flow initiation	3	30	1	1	16.155	10.992	47.0	1.561
g25t12	flow initiation	3	30	1	10	16.107	10.985	46.6	1.560
g25t13	flow initiation	3	30	1	100	15.654	10.918	43.4	1.551
g25t14	flow initiation	3	30	1	1000	14.144	10.330	36.9	1.474